Cell Calcium 57 (2015) 263–274

Contents lists available at ScienceDirect

Cell Calcium

journal homepage: www.elsevier.com/locate/ceca

# Fluorescent biosensors illuminate calcium levels within defined beta-cell endosome subpopulations

Tobias Albrecht[a,1], Yongxin Zhao[b,1], Trang Hai Nguyen[b], Robert E. Campbell[b], James D. Johnson[a,*]

[a] Department of Cellular and Physiological Sciences, University of British Columbia, Vancouver, BC, Canada
[b] Department of Chemistry, University of Alberta, Edmonton, AB, Canada

ARTICLE INFO

*Article history:*
Received 11 July 2014
Received in revised form
26 December 2014
Accepted 19 January 2015
Available online 28 January 2015

*Keywords:*
Endosome
Fluorescence imaging
$Ca^{2+}$ biosensor
pH biosensor
Pancreatic beta-cell
Glucose

ABSTRACT

Live cell imaging has revealed that calcium ions ($Ca^{2+}$) pass in and out of many cellular organelles. However, technical hurdles have limited measurements of $Ca^{2+}$ in acidic organelles, such as endosomes. Although evidence hints that endosomes play a role in $Ca^{2+}$ signaling, direct measurements within endosomal lumina represent one of the final frontiers in organelle imaging. To measure $Ca^{2+}$ in a TiVAMP-positive endosome sub-population, the pH-resistant ratiometric $Ca^{2+}$ biosensor GEM-GECO1 and the ratiometric pH biosensor mKeima were used. A positive correlation between acidic endosomal pH and higher $Ca^{2+}$ was observed within these Rab5a- and Rab7-positive compartments. $Ca^{2+}$ concentration in most endosomes was estimated to be below 2 μM, lower than $Ca^{2+}$ levels in several other intracellular stores, indicating that endosomes may take up $Ca^{2+}$ during physiological stimulation. Indeed, endosomes accumulated $Ca^{2+}$ during glucose-stimulation, a condition where endosomal pH did not change. Our biosensors permitted the first measurements revealing a role for endosomes in cellular $Ca^{2+}$ homeostasis during physiological stimulation.



## 1. Introduction

Calcium ions ($Ca^{2+}$) play many essential roles in cellular signaling. The plasma membrane separates the low cytoplasmic $Ca^{2+}$ concentration (<200 nM in a quiescent cell) from the much higher extracellular $Ca^{2+}$ levels (>1 mM). Multiple organelles participate in global cellular $Ca^{2+}$ homeostasis, while also signaling locally to regulate specific subcellular events [1–3]. Fluorescent protein-based biosensors enable direct measurements of $Ca^{2+}$ dynamics within the lumina of defined $Ca^{2+}$ handling organelles, and provide minimally invasive windows into their respective roles in cellular physiology [4]. Some organelles function primarily as $Ca^{2+}$ stores, whereas other organelles are transient $Ca^{2+}$ buffers that act to shape cellular $Ca^{2+}$ signals and protect cells from excitotoxicity [1]. The endoplasmic reticulum (ER) is the most well characterized intracellular $Ca^{2+}$ store, with $Ca^{2+}$ levels of 250–600 μM [5]. ER $Ca^{2+}$ concentration is primarily regulated by $Ca^{2+}$-importing pumps called sarco/endoplasmic reticulum $Ca^{2+}$-ATPases (SERCAs), as well as $Ca^{2+}$ release channels including the $IP_3R$ and RyR [1,6]. The Golgi network also stores $Ca^{2+}$ (100–300 μM) at levels that facilitate post-translational protein modifications [7,8]. On the other hand, direct measurements in living cells indicate that other organelles, such as the nucleus and mitochondria, rapidly take up $Ca^{2+}$ but do not act as long-term stores for significant amounts of $Ca^{2+}$ [1]. Roles in $Ca^{2+}$ handling have been proposed for other organelles, particularly the acidic organelles of the endosomal and lysosomal systems [9], but direct and specific measurements of $Ca^{2+}$ within those lumina have been challenging due to the disproportionate pH sensitivity of existing $Ca^{2+}$ biosensors [10]. Thus, despite the fact that endosomes are important signaling organelles [11], the physiological role of endosomal $Ca^{2+}$ fluxes remains poorly understood.

The highly acidic nature of endosomes dictates that biosensors with sufficient pH insensitivity are required for luminal $Ca^{2+}$ imaging in this compartment. Although current Förster resonance energy transfer (FRET)-based 'cameleon' probes are acceptable for ER and other organelles [6,12,13], they are large (>70 kDa) and typically incorporate highly pH-sensitive fluorescent protein variants that are quenched in acidic environments. Single fluorescent protein $Ca^{2+}$ biosensors (*e.g.* G-CaMP) [14,15] are smaller, but

* Corresponding author at: Life Sciences Institute Diabetes Research Group, Department of Cellular and Physiological Sciences, University of British Columbia, 5358 Life Sciences Building, 2350 Health Sciences Mall, Vancouver, BC V6T 1Z3, Canada. Tel.: +1 604 822 7187; fax: +1 604 822 2316.
*E-mail address:* James.D.Johnson@ubc.ca (J.D. Johnson).
[1] These authors contributed equally to this work.

http://dx.doi.org/10.1016/j.ceca.2015.01.008

**Table 1**
The $K_d$, Hill coefficient $n$, $R_{max}$ and $R_{min}$ of GEM-GECO1 obtained from fitting at different pH values.

| pH | $K_d$ (mM) | $n$ | $R_{max}$ | $R_{min}$ | Adjusted $R^2$ |
|---|---|---|---|---|---|
| 4.97 | 54.24 | 2.80 | 0.954 | 0.050 | 0.999 |
| 5.42 | 17.88 | 2.97 | 1.402 | 0.050 | 0.999 |
| 6.00 | 3.09 | 2.70 | 1.533 | 0.041 | 0.999 |
| 6.50 | 0.68 | 2.75 | 1.418 | 0.035 | 0.999 |
| 7.00 | 0.46 | 3.02 | 1.453 | 0.017 | 0.996 |
| 7.50 | 0.27 | 2.27 | 1.476 | 0.021 | 0.998 |

also typically employ pH-sensitive fluorescent proteins [14,16]. Recently, we developed an expanded series of $Ca^{2+}$ indicators *via* directed evolution of G-CaMP3 [16]. One variant in this series, known as GEM-GECO1, exhibits a blue-green ratiometric emission, a $K_d$ of 340 nM, an exceptionally high dynamic range (11,000% change *in vitro*), and is relatively pH insensitive [16]. Specifically, GEM-GECO1 still maintains 50% of its maximum dynamic range at the acidic pH of 6.1, and we therefore considered that it might be suitable for $Ca^{2+}$ imaging in endosomes of living cells.

Here, we describe the combined use of GEM-GECO1 and a pH biosensor to achieve calibrated and pH-corrected, semi-quantitative $Ca^{2+}$ measurements in the endosomal lumen. Using this novel approach, we estimated the baseline $Ca^{2+}$ concentration of Rab5a- and Rab7-positive endosomes and imaged the kinetics of endosomal $Ca^{2+}$ fluxes in glucose-stimulated beta-cells. Using this new tool, we discovered that endosomes take up $Ca^{2+}$ in glucose-stimulated beta-cells.

## 2. Materials and methods

### 2.1. Cloning, plasmids and transfection

Synthetic DNA oligonucleotides used for cloning and library construction were purchased from Integrated DNA Technologies (Coralville, Iowa). The sequences of all oligonucleotides used in this work are provided in Table 2. Pfu polymerase (Fermentas, Waltham, MA) and Pfx polymerase (Life Technologies, Carlsbad, CA) were used for non-mutagenic PCR amplifications in the buffer supplied by the respective manufacturer. PCR products and products of restriction digests were routinely purified using preparative agarose gel electrophoresis followed by DNA isolation using the GeneJET Gel Extraction Kit (Fermentas) and MinElute Gel Extraction Kit (Qiagen, Hilden, Germany). Restriction endonucleases were purchased from Fermentas and New England Biolabs (Ipswich, MA) and were used according to the manufacturers' recommended protocol. Ligations were performed using T4 ligase in Ligation Buffer (Life Technologies, New England Biolabs). Small-scale isolation of plasmid DNA was performed using the GeneJET Miniprep Kit (Fermentas) and QIAprep Spin Miniprep Kit (Qiagen). Invitrogen's PureLink HiPure Plasmid Filter Maxiprep Kit was used for large scale DNA amplification.

MIN6 beta-cells were cultured in DMEM media containing 25 mM glucose (Sigma–Aldrich, St. Louis, MO) supplemented with 10% (v/v) FBS (Life Technologies) and penicillin/streptomycin (100 μg/ml; Life Technologies) at 37 °C and 5% $CO_2$ as described previously [6]. All constructs were transfected into MIN6 cells using the NEON Transfection system. 2 μg of plasmid DNA were used to electroporate 1 million MIN6 cells. Cells were electroporated with two 1200 V pulses with a pulse width of 20 ms.

Primary hand picked human islets from a healthy 11-year-old male donor were dispersed and electroporated using the NEON transfection system (2 μg DNA per 1 million cells, 1000 V, 2 pulses, 30 ms pulse width) and subsequently cultured in CMRL medium for 72 h prior imaging.

### 2.2. Microscopy and image analysis

Colocalization images were acquired using a widefield inverted Zeiss Axiovert 200M microscope equipped with a 100× 1.45NA objective. Image stacks were deconvolved using Slidebook Software to obtain confocal image planes. Object based colocalization studies were performed using the Fiji/ImageJ plugin JaCoP [17].

Live cell imaging of MIN6 and primary cells was performed on a wide-field microscope setup (Zeiss Axiovert 200M) with a mounted 40× Plan-NeoFluar 1.3NA oil objective (Zeiss, Jena, Germany) [6]. Cells were cultured and imaged on poly-D-lysine coated No. 1.5 25 mm circular borosilicate coverslips (Electron Microscopy Sciences, Hatfield, PA) and were kept at 37 °C in a temperature controlled incubation chamber (Harvard Apparatus, Holliston, MA) during imaging. Images were acquired with a CoolSNAP HQ2 CCD camera (Photometrics, Tucson, AZ). GEM-GECO1 was excited with a selective bandpass filter (386/23 nm) and emissions were detected with selective bandpass filters (440/40 nm and 520/32 nm) using a single filter cube with a mounted dichroic mirror. The Sutter Lambda 10-2 emission filter wheel is capable of switching between different emission filters within 75 ms. Ratiometric mKeima imaging was performed by using selective excitation filters (430/25 nm and 575/50 nm) and a 632/60 nm emission filter. The excitation filters were mounted in a Sutter instruments DG4 light source enabling excitation switches in <2 ms. The exposure times for GEM-GECO1 and mKeima detection were kept at ≤1 s.

Sensor calibration imaging of purified GEM-GECO1 and mKeima protein was performed in a 96 well-plate with a No. 1.5 glass bottom. The calibration is detailed below. Time-lapse image sequences, as well as still images, were analyzed using Slidebook software (Intelligent Imaging Innovations, Denver, CO), Cell Profiler 2.0 [18], and the ImageJ distribution Fiji [19]. Local background subtraction was performed to correct for cellular autofluorescence [20]. Live-cell experiments were performed with preheated solutions and stable perfusion at 1 ml/min, and complete solution changes were achieved in <60 s. Live cells were imaged in Ringer's buffer (119 mM NaCl, 4.7 mM KCl, 25 mM $NaHCO_3$, 2.5 mM $CaCl_2$, 1.2 mM $MgSO_4$, 1.2 mM $H_2PO_4$) supplemented with glucose as indicated in the figures.

### 2.3. Protein purification and in vitro spectroscopy

To purify GEM-GECO1 for *in vitro* spectroscopic characterization, the pBAD plasmid harboring the gene for mKeima–GEM-GECO1 was first used to transform electrocompetent *E. coli* DH10B cells. Following selection on LB/ampicillin (200 mg/ml), single colonies were picked and used to inoculate 4 mL LB medium (200 mg/ml ampicillin, 0.2% L-arabinose). Bacterial cultures were shaken at 250 rpm and allowed to grow for 30 h at 30 °C. Bacteria were harvested by centrifugation (10,000 × *g* for 5 min), resuspended in 30 mM Tris–HCl buffer (pH 7.4), lysed by French press, and clarified by centrifugation at 13,000 × *g* for 45 min at 4 °C. Proteins were purified from the cell-free extract by Ni-NTA affinity chromatography (Agarose Bead Technologies, Tampa, FL). Purified proteins were dialyzed into either 30 mM Tris, 150 mM NaCl, pH 7.4 or 10 mM MOPS, 100 mM KCl, pH 7.2. Fluorescence spectra were recorded on a Safire2 plate reader (Tecan, Maennedorf, Switzerland). Since GEM-GECO1 and mKeima are ratiometric sensors, the response to $Ca^{2+}$ or $H^+$ is expressed as the fluorescent ratio *R*. For GEM-GECO1, *R* = (*I* at 453 nm)/(*I* at 513 nm), where *I* = fluorescence intensity when excited at 390 nm. For mKeima *R* = (*I* with 584 nm excitation)/(*I* with 448 nm excitation), where *I* = fluorescence intensity at 635 nm.

**Table 2**
Primers used in this study.

| Primer name | Primer sequence (5′–3′) |
|---|---|
| Fw_NcoI_6xhis_mKeima | GCGATGCCATGGGTCATCATCATCATCATCATGGTACAATGGTCGACTCTAGAATGGTGAGTGTGATCGCTAAACAAATGACC |
| Rv_mKeima_KpnI_HindIII | GCGAAAGCTTCTATCCGGTACCCATGGTACTTCCACCTGTGCCACC |
| Fw_KpnI_GEM | GCGAGGTACCACCATGGTCGACTCATCACGTC |
| Rv_GECO-Stop-HindIII | GCGATGAAGCTTCTACTTCGCTGTCATCATTTGTACAAACTCTTCGTAGTTT |
| Fw_ApaI_TiVAMP | GGGGGCCCGCCGCCATGGCGATTCTTTTTGCTGTTGTTG |
| Rv_TiVAMP_NotI | CGCGGCCGCTTTCTTCACACAGCTTGGCCATG |
| Fw_EcoRI_GEM-GECO1 | CGAATTCTAACGCCGCGACGTGCGACTGCG |
| Rv_GEM-GECO1_HindIII | CAAGCTTCTACTTCGCTGTCATCATTTGTACAAAC |
| Fw_XbaI_mKeima | CCTCTAGAATGGTGAGTGTGATCGCTAAACAAATGACCTACAAGG |
| Rv_mKeima_HindIII | GGAAGCTTCTAACCGAGCAAAGAGTGGCGTGCAATGG |
| Fw_SacI_Rab5a | GGCGAGCTCAAATGGCTAGTCGAGGCGCAACAAG |
| Rv_Rab5a_BamHI | CGCGGATCCTTACAGATCCTCTTCTGAGATGAGTTTC |
| Fw_SacI_Rab7 | GGCGAGCTCAAATGGGCAGCCGCGACCACCTG |
| Rv_Rab7_BamHI | CGCGGATCCTTACAGATCCTCTTCTGAGATGAGTTTC |

### 2.4. Determination of $K_a$ of mKeima as a pH indicator

mKeima was used as an organelle pH indicator. To achieve this, we needed to measure the apparent $pK_a$ of mKeima using standard solutions with different pHs, prepared as follows. A solution containing 30 mM trisodium citrate and 30 mM borax was adjusted to pH 11.5 and HCl (12 M and 1 M) was then added drop-wise to provide solutions with pH values ranging from 11.5 to 3 in 0.5 pH unit intervals. In a 96-well plate, 1 μl of concentrated mKeima protein solution in MOPS buffer (30 mM MOPS, 100 mM KCl, at pH 7.2) was added into a well containing 100 μl of each of the standard solutions described above. The mKeima fluorescence in each pH condition was recorded using a Safire2 multiwell fluorescence plate reader, with three replicates. The results were fitted in the following Hill equation:

$$R_{\text{mKeima}} = 0.106 - \frac{3.18 \times [\text{H}^+]^{1.16}}{[\text{H}^+]^{1.16} + 1.89 \times 10^{-7}} \quad (1)$$
$$R^2 = 0.993$$

### 2.5. Determination of $Ca^{2+}$ $K_d$ of GEM-GECO1 at different pHs

The $K_d$ of GEM-GECO1 as a function of the pH can be determined by $Ca^{2+}$ titrations in a series of standard solutions at different pHs values. $Ca^{2+}$ titrations were performed by dilution (1:100) of a concentrated protein solution of mKeima–GEM-GECO1 into a series of buffers which were prepared by mixing $Ca^{2+}$-saturated and $Ca^{2+}$-free buffers (30 mM MOPS, 100 mM KCl, 10 mM EGTA, either with or without 10 mM $Ca^{2+}$) in different ratios to provide a series of solutions with various free $Ca^{2+}$ concentration at 20 °C [21].

To determine the $K_d$ of GEM-GECO1 as a function of pH, we prepared a series of buffers with different pH values (pH 5, 5.5, 6.0, 6.5, 7.0 and 7.5). Each pH buffer was prepared as a $Ca^{2+}$-saturated and a $Ca^{2+}$-free solution. We then used these standard solutions to mix more buffers with various $Ca^{2+}$ concentrations for each given pH. Since the $K_d$ values of the Ca–EGTA complex in different conditions are known, we can calculate the free $Ca^{2+}$ concentration in each buffer. Note that the pH and ionic strength of the buffer must be taken into account, as they influence the $K_d$ of the Ca–EGTA complex. Free $Ca^{2+}$ at different pHs, ionic strengths and different ratios of Ca–EGTA to EGTA can be conveniently calculated using MaxChelator (http://www.stanford.edu/~cpatton/maxc.html) [22]. For a series of $Ca^{2+}$ buffers at a given pH, the fluorescence ratio of GEM-GECO1 in each solution ($Ca^{2+}$-free and $Ca^{2+}$-saturated) was measured in the fluorescence plate reader and plotted as a function of $Ca^{2+}$ concentration (Fig. 4A). Experiments were performed in triplicate and the averaged data from the three independent measurements was fit to the Hill equation to calculate effective $K_d$ value of GEM-GECO1 at that given pH (Table 1). The $K_d$ values obtained from different pHs were then used to determine the $K_d$ as the function of $H^+$ concentration was fit to a parabolic equation to obtain:

$$K_d(\text{H}^+) = 1.55 \times 10^{11} \times [\text{H}^+]^2 + 3.47 \times 10^6 \times [\text{H}^+] + 0.019 \quad (2)$$
$$R^2 = 0.98$$

Because the chromophore environment in $Ca^{2+}$-unbound and bound states of GEM-GECO1 is also influenced by the pH, the maximum and minimum ratios ($R_{max}$ and $R_{min}$) of GEM-GECO1 are also dependent on the pH and require calibration. $R_{max}$ and $R_{min}$ from the fitted equations in different pHs were extracted and fit to the Hill equations in order to establish the relationship between $R_{max}$ and $R_{min}$ and pH. This procedure provided the following equations:

$$R_{\text{max}}(\text{H}^+) = 1.46 - \frac{1.36 \times [\text{H}^+]^{2.86}}{[\text{H}^+]^{2.86} + 9.93 \times 10^{-15}} \quad (3)$$
$$R^2 = 0.89$$

$$R_{\text{min}}(\text{H}^+) = 0.020 + \frac{0.031 \times [\text{H}^+]^{1.41}}{[\text{H}^+]^{1.41} + 1.53 \times 10^{-15}} \quad (4)$$
$$R^2 = 0.98$$

By substituting $K_d$, $R_{max}$ and $R_{min}$ using Eqs. (1), (3) and (4) respectively, the final calibration equation could be generalized as followed:

$$R_{\text{GEM-GECO1}}(\text{H}^+) = R_{\text{min}}(\text{H}^+) + [R_{\text{max}}(\text{H}^+) - R_{\text{min}}(\text{H}^+)] \times \frac{[\text{Ca}^{2+}]_{\text{free}}^{2.85}}{[K_E(\text{H}^+)^{2.85} + [\text{Ca}^{2+}]_{\text{free}}^{2.85}]} \quad (5)$$

where the Hill coefficient ($n = 2.85$) is the average of Hill coefficients of the fitted equations for pH 5.0–7.0. Eq. (5) can be further reordered into Eq. (6):

$$[\text{Ca}^{2+}]_{\text{free}} \approx K_d(\text{H}^+) \times \left[\frac{R_{\text{GEM-GECO1}}(\text{H}^+) - R_{\text{min}}(\text{H}^+)}{R_{\text{max}}(\text{H}^+) - R_{\text{GEM-GECO1}}(\text{H}^+)}\right]^{0.35} \quad (6)$$

Eq. (6) is the function for the 3-dimensional surface plot of the response of GEM-GECO1 as a function of $Ca^{2+}$ concentration and pH *in vitro* shown in Fig. 4C).

### 2.6. Conversion of mKeima and GEM-GECO1 ratios into estimated pH and free $Ca^{2+}$ level in situ

With Eq. (6) and the correlated $R_{max}$ and $R_{min}$ of mKeima and GEM-GECO1, the signals of mKeima and GEM-GECO1 obtained from *in situ* experiments were translated into the estimated pH and $Ca^{2+}$ levels in endosomes. Briefly, the estimated pH was calculated based on the raw ratio of mKeima using Eq. (1). The estimated pH

was then used to determine the $K_d$, $R_{max}$ and $R_{min}$ of GEM-GECO1. Finally, the free $Ca^{2+}$ concentration was calculated based on the raw ratio of GEM-GECO1, the calculated $K_d$, the calculated $R_{max}$, and the calculated $R_{min}$, by using Eq. (6). In these images, 33 out of 230 measured endosomes were below the minimum fluorescent GEM-GECO1 ratio ($R_{min}$) due to an insufficient signal to noise ratio and were excluded from the following conversion.

After the conversion, we obtained (semi)quantitative information of $Ca^{2+}$ levels of endosomes with different pHs which reveals a clear correlation between the $Ca^{2+}$ level and the pH of endosomes. In contrast, the raw signal ratios of mKeima and GEM-GECO1 were poorly correlated (Fig. 5B). To address the reliably of our data, we estimated the upper and lower limit of quantification using the confidence band (95%) of the $Ca^{2+}$ titration curves with different pHs according to literature [52]. Subsequently, we fit the upper and lower limit of quantification using equation $y = a \cdot b^{pH}$. The results are plotted in Fig. 5D. In addition, we also give the 95% confidence band for the fitted curves in Fig. 5D. As shown in Fig. 5D, red and blue lines indicate the upper and lower limit of quantification, the dash lines represent the 95% confidence band. These lines define the usable range for measuring $Ca^{2+}$ concentration using GEM-GECO1 under different pHs. Within the endosomal pH (below 6.5), most of the data points and the regression curve fall within the valid region, which demonstrates that our measurements are statically valid.

### 2.7. Statistical analysis

Data are expressed as mean ± SEM. Statistical analysis throughout the study was performed by applying two-tailed student *t*-tests. Significance was defined at $p < 0.05$.

## 3. Results

### 3.1. TiVAMP–GEM-GECO1 is a luminal $Ca^{2+}$ biosensor localized to early and late endosomes

To generate an endosomal lumen targeted $Ca^{2+}$ biosensor, tetanus-insensitive vesicle-associated membrane protein (TiVAMP, also known as VAMP7) was used as a targeting protein. TiVAMP is a SNARE protein that drives endosomal fusion and is known to be localized to endosomes [23–25]. The functional domain responsible for membrane tethering is located at the cytoplasmic N-terminus of TiVAMP [26]. It has been previously reported that C-terminal tagging of TiVAMP leads to a functional protein with the tethered fusion partner localized to the endosomal lumen [26]. GEM-GECO1 was fused to the C-terminus of TiVAMP–GEM-GECO1 *via* a 61 amino acid linker that was included to mitigate functional interference with its fusion partners (Fig. 1A). Fluorescence imaging of MIN6 beta-cells transfected with a vector encoding TiVAMP–GEM-GECO1 revealed that the protein product localized to endosome-like structures and exhibited fluorescence emission that was much brighter than the background autofluorescence (Fig. 1B and C). To validate the proper localization of TiVAMP–GEM-GECO1, we co-expressed the sensor with markers of specific endolysosomal compartments. The endosomal calcium sensor colocalized with red fluorescent markers for early endosomes (TagRFP-Rab5a, Fig. 1 D), late endosomes (TagRFP-Rab7, Fig. 1E) and Lysotracker, a tracer dye for acidic vesicles (Fig. 1F). By this colocalization analysis, we observed that ~70% of the TiVAMP–GEM-GECO1-positive endosomal population is marked by Rab5a (23%), Rab7 (24%) or Lysotracker (22%). The remaining minority of ~30% TiVAMP–GEM-GECO1 likely localized to endosomal compartments that are not labeled in this analysis (*e.g.* recycling endosomes). Taken together with the known cellular localization of TiVAMP, these data confirm that the $Ca^{2+}$ biosensor TiVAMP–GEM-GECO1 localizes to both early and late endosomes in beta-cells.

### 3.2. TiVAMP–GEM-GECO1 senses endosomal $Ca^{2+}$ changes in the physiological range

We next examined the functionality of TiVAMP–GEM-GECO1. First, we simply modified endosomal $Ca^{2+}$ by changing the $Ca^{2+}$ content of the extracellular media entering MIN6 cells transfected with TiVAMP–GEM-GECO1. A switch from $Ca^{2+}$-free media to standard media containing 2 mM $Ca^{2+}$ significantly increased the endosomal $Ca^{2+}$ concentration detected with TiVAMP–GEM-GECO1. Conversely, endosomal $Ca^{2+}$ was reduced by incubating cells in buffer containing 0 mM $CaCl_2$ or 1 mM of the $Ca^{2+}$ chelator EGTA, compared with standard 2 mM $CaCl_2$ (Fig. 2A and B). These data suggest that TiVAMP–GEM-GECO1 can reflect changes in extracellular $Ca^{2+}$, possibly due to the simple fluid phase endocytosis of extracellular media.

Dynamic changes in endosomal $Ca^{2+}$ were assessed with time-lapse imaging. TiVAMP–GEM-GECO1-transfected MIN6 cells were initially incubated in standard 2 mM $CaCl_2$ Ringer's solution, after which this baseline solution was replaced with a high $Ca^{2+}$ (20 mM $CaCl_2$) Ringer's solution containing ionomycin to promote $Ca^{2+}$ flux across membranes. As expected, endosomal $Ca^{2+}$ levels increased significantly compared to baseline (Fig. 2C). Subsequently, the elevated endosomal $Ca^{2+}$ was depleted by perfusion of the cells with $Ca^{2+}$ free Ringer's solution containing ionomycin and 1 mM EGTA. The TiVAMP–GEM-GECO1 biosensor reflected this change with a change in the emission ratios, which corresponded to a lower relative $Ca^{2+}$ concentration compared to baseline (Fig. 2C). Note that the baseline emission ratio for endosomal $Ca^{2+}$ is between the maximum and minimum ratios obtained during this experiment. This maximum-minimum pattern of TiVAMP–GEMCO1 could be observed both in averages of all endosomes within a cell, as well as with analysis of populations of single endosomes (Fig. 2C and D). Taken together, these data suggest that TiVAMP–GEM-GECO1 dynamically reports luminal $Ca^{2+}$ changes in endosomes and that it has adequate dynamic range to sense changes in luminal $Ca^{2+}$ in these specific compartments.

### 3.3. Endosomes enrich $Ca^{2+}$ during maturation

During the course of our experiments, we observed a remarkable heterogeneity in $Ca^{2+}$ levels in the total pool of TiVAMP–GEM-GECO1 labeled endosomes (Fig. 2D). Single endosome population analysis of MIN6 cells bathed in standard 2 mM $CaCl_2$ buffer revealed that $Ca^{2+}$ levels varied dramatically between endosomes within a single cell (Fig. 3A–D). While this heterogeneity can be caused to some degree by the movement of the vesicle between the acquisitions of the individual channels during ratiometric imaging, we still observed remarkable differences in fluorescent ratios by observing individual vesicles (Fig. 3D). We therefore tested the hypothesis that this heterogeneity in luminal $Ca^{2+}$ levels was associated with the maturation of endosomes toward the lysosomal compartment [27]. Indeed, by analyzing only endosomes labeled with TagRFP-Rab5a and TiVAMP–GEM-GECO1, we found a lower relative endosomal $Ca^{2+}$ concentration in early endsomes compared to late endosomes labeled by TagRFP-Rab7 and TiVAMP–GEM-GECO1 (Fig. 3E and F). The increase in luminal $Ca^{2+}$ composition of endosomes as they mature and fuse with lysosomes is consistent with the process of endosomal acidification during the transport of the organelle to lysosomes, which is thought to increase the driving force for $Ca^{2+}$ uptake [28]. Collectively, our data suggest that $Ca^{2+}$ in TiVAMP-labeled endosomes increases

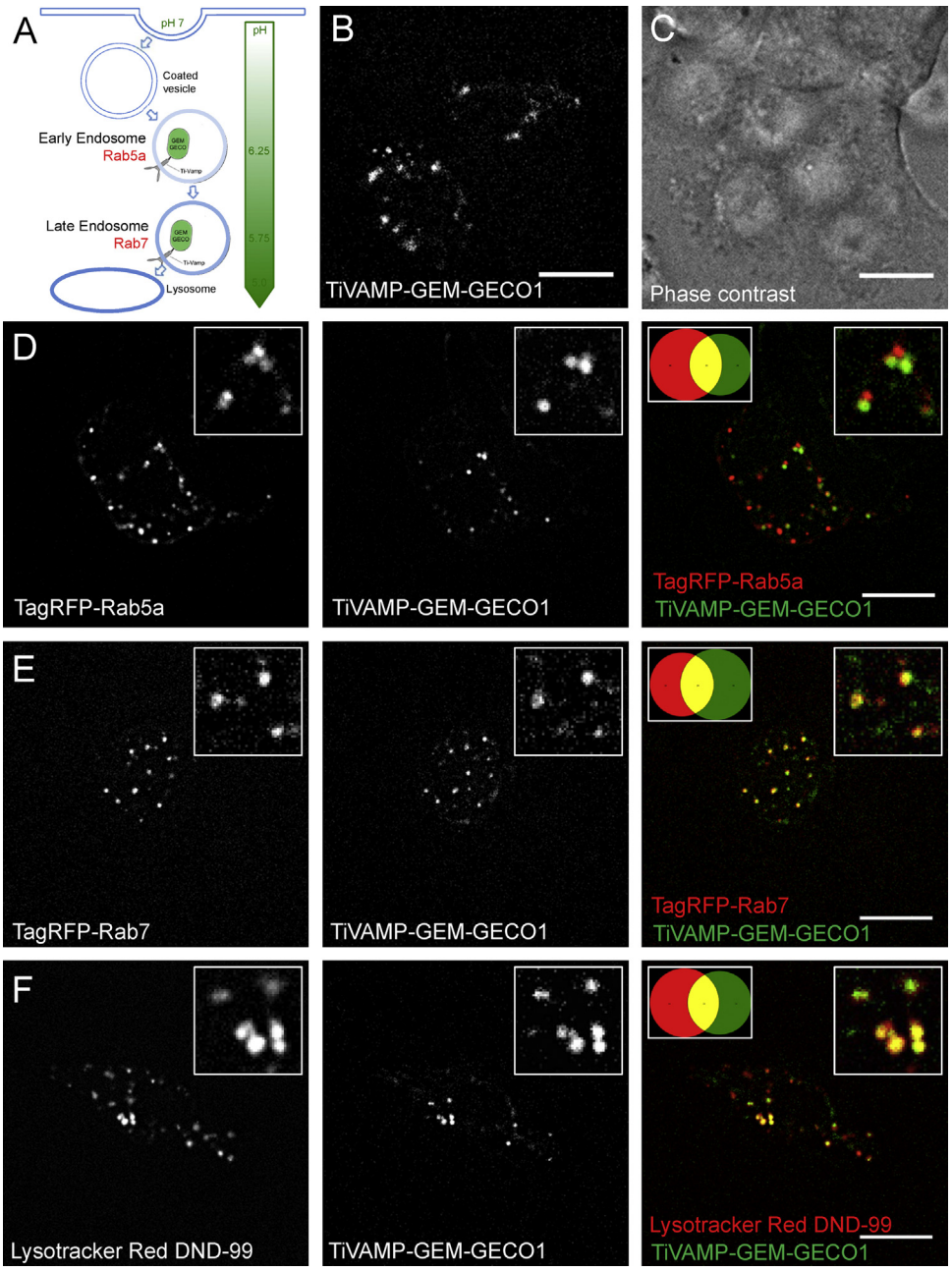


**Fig. 1.** TiVAMP localizes to early and late endosomes. (A) Schematic illustration of the specific targeting of GEM-GECO1 to the endosomal lumen, as well as the pH gradient along the endolysosomal pathway established from the literature. Note that the very earliest vesicle after endocytosis is not likely to be tagged with the $Ca^{2+}$ or pH sensor probes. (B, C) Expression of TiVAMP–GEM-GECO1 in MIN6 cells, shown in fluorescence and phase contrast modes. (D) TiVAMP–GEM-GECO1 colocalizes with early endosomes labeled by TagRFP-Rab5a. (E) TiVAMP–GEM-GECO1 colocalizes with TagRFP-Rab7-positive late endosomes. (F) TiVAMP–GEM-GECO1 colocalizes to acidic vesicles labeled by the tracer dye Lysotracker Red DND-99. Representative images are shown. Scale bar equals 10 μm. Inset Venn diagrams visualize the degree of vesicle colocalization obtained by object based colocalization analysis ($n = 10$ cells for each condition).

during the maturation from Rab5a-positive 'early' endosomes to Rab7-positive 'late' endosomes.

### 3.4. Semi-quantitative $Ca^{2+}$ measurements and in vitro calibration

From the above results, it was apparent that TiVAMP–GEM-GECO1 could qualitatively report on endosomal $Ca^{2+}$ dynamics. However, to achieve semi-quantitative interpretation of the GEM-GECO1 emission ratio, we required a means of accounting for differences in both $Ca^{2+}$ and pH in single endosomes. Endosomes are challenging organelles for semi-quantitative approaches since their luminal composition is highly dynamic [28]. In addition, both the maximal fluorescence response and the $Ca^{2+}$ dissociation constant ($K_d$) of GEM-GECO1 are dependent on pH (Fig. 4A), despite the improved pH resistance of this biosensor when compared to other $Ca^{2+}$ sensors [16]. To achieve semi-quantitative pH measurements, we employed mKeima, a fluorescent protein that is known to have pH-dependent excitation peaks at 440 nm and 590 nm ($pK_a = 6.0$) [29,30], making it a suitable ratiometric pH biosensor. Indeed, *in vitro* measurements of the excitation ratio of mKeima at different pH values showed a strong dependence between pH values of 5 and 6 (Fig. 4B). To determine the apparent $pK_a$ for mKeima, a series of pH buffers was prepared. The fluorescence of mKeima

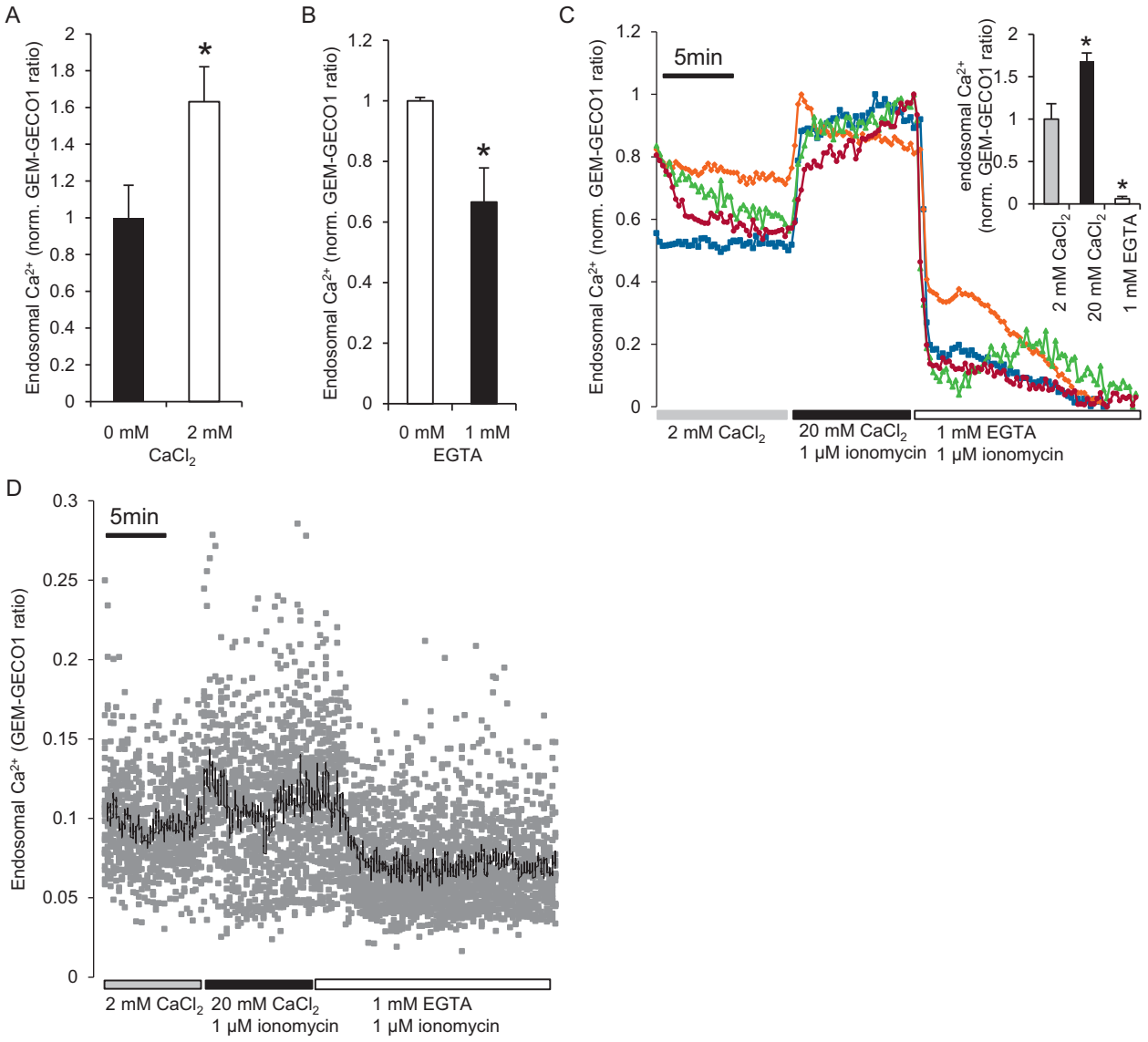


**Fig. 2.** TiVAMP–GEM-GECO1 senses changes in endosomal $Ca^{2+}$. (A, B) Endosomal $Ca^{2+}$ was modified by fluid phase internalization of Ringer's buffer of different compositions. (A) MIN6 cells were incubated for 30 min with either $CaCl_2$ free or 2 mM $CaCl_2$ containing Ringer's. (B) Extracellular calcium of 2 mM $CaCl_2$ Ringer's was chelated by incubating cells for 30 min with 1 mM EGTA and compared to cells incubated in regular Ringer's media containing 2 mM $CaCl_2$. The bar graphs represent averaged endosomal GEM-GECO1 ratios per cell ($n = 4$). (C) Live-cell perfusion demonstrates the responsiveness and dynamic range of TiVAMP–GEM-GECO1 to induced changes in endosomal $Ca^{2+}$ content (averaged per cell). Inset graph shows a 1-min average of endosomal GEM-GECO1 ratios at the end of each individual treatment as a fold change to the baseline to demonstrate the significant change in GEM-GECO1 ratios caused by the treatment ($n = 4$). (D) GEM-GECO1 ratio analysis of the population of single endosomes per time point in one cell in response to indicated treatments in a live cell perfusion experiment. The black line represents the average endosomal $Ca^{2+}$ content at each time point. $^*p < 0.05$, error bars represent SEM.

in each buffer condition was recorded. The results were fit to a Hill equation to calculate the effective $K_a$ of mKeima. The apparent $pK_a$ of mKeima measured in our studies was 5.80.

It is not currently technically possible to simultaneously clamp both pH and $Ca^{2+}$ within both endosomal and cytosolic compartments, which precluded attempts at *in situ* calibration. Thus, we employed an *in vitro* approach to calibrate the probe combination of GEM-GECO1 and mKeima. A tandem protein composed of GEM-GECO1 fused to mKeima *via* a 14 amino acid residue linker (GGTGGSTMGTMVD) displayed the dynamic and spectral sensing properties of each of the single biosensors. Although it was not useful in living cells, it was ideal for generating a calibration curve essential for quantitative imaging of both $Ca^{2+}$ and pH. To determine the $K_d$ of GEM-GECO1 as a function of pH, we prepared a series of $Ca^{2+}$-saturated and $Ca^{2+}$-free buffers at different pH values. For a series of pHs, the fluorescence ratio of GEM-GECO1 in each solution was determined using a multi-well plate reader, and plotted as a function of $Ca^{2+}$ concentration (Fig. 4A). These data were fit to the Hill equation to calculate effective $K_d$ value of GEM-GECO1 at that given pH (Table 1 and Fig. 4C). The fluorescence of these samples was also measured on the microscope stage using the same filter sets as used for cell imaging experiments. The maximum and minimum ratios of mKeima and GEM-GECO1 obtained in the microscope measurements were used to substitute for the corresponding parameters of the fitting equations (Fig. 4H–J). For the microscope calibration, we assumed that the $K_d$ and Hill coefficient are identical to the previously measured values, and so the only parameters that needed to be adjusted were the maximum and minimum signal ratios ($R_{max}$, $R_{min}$) of mKeima and GEM-GECO1. To test this assumption, we analyzed the intensity ratios of pure mKeima protein in MOPS buffer measured *in vitro* and the data obtained from imaging the GEM-GECO1-mKeima solutions at the microscope. The fitting

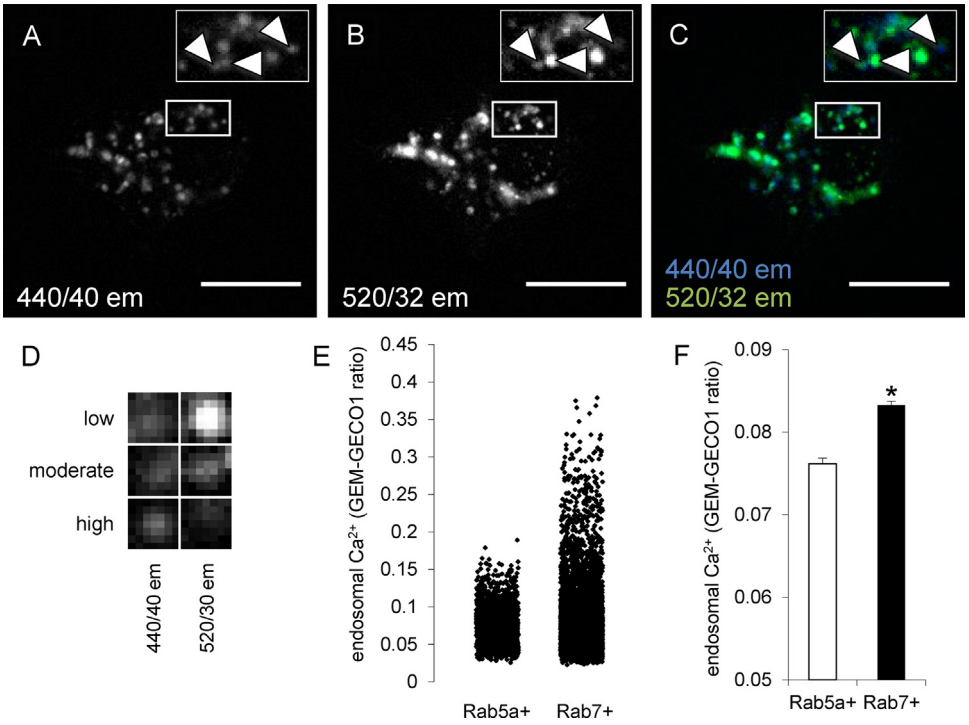


**Fig. 3.** $Ca^{2+}$ enrichment of endosomes during maturation. (A–D) Heterogeneity in relative endosomal $Ca^{2+}$ content in a MIN6 cell visualized with TiVAMP–GEM-GECO1. Arrowheads point to endosomes with different luminal $Ca^{2+}$ contents. (E, F) Analysis of relative single endosome $Ca^{2+}$ content of early, Rab5a labeled and late, Rab7 labeled endosomes (8 cells). $^{*}p < 0.05$, error bars represent SEM, >1600 endosomes analyzed per population.

equations of all conditions were similar, with the primary difference between the experimental values of $R_{max}$ and $R_{min}$ (Fig. 4D–F,). Moreover, the values for $pK_a$ and Hill coefficients showed no significant difference between the calibrated measurements (Fig. 4E and F; $p > 0.1$). The calibration equations obtained through the procedure described above enabled the estimation of endosomal pH and $Ca^{2+}$ using the emission ratios obtained from GEM-GECO1 and mKeima (Fig. 4G).

### 3.5. Semi-quantitative endosomal $Ca^{2+}$ and pH measurement in living cells

To generate a probe for pH monitoring in endosomes, we fused mKeima to TiVAMP to enable endosomal pH measurements. TiVAMP–mKeima was co-expressed with TiVAMP–GEM-GECO1 for quantitative $Ca^{2+}$ imaging in live cells (Fig. 5A). As expected, the biosensors TiVAMP–GEM-GECO1 and TiVAMP–mKeima colocalized in the same organelles (Fig. 5A). By co-expression of both biosensors, we were able to determine the mean intensity ratios for both mKeima and GEM-GECO1 within individual endosomes (Fig. 5B). To support our measurements, we modeled contour curves of fixed $Ca^{2+}$ concentrations in the diagram (Fig. 5B). These lines indicate that our measurements are within the detection range of the sensor pair, since the GEM-GECO1 ratio is only robustly affected by changes within the endosomal pH range at rather high $Ca^{2+}$ concentrations (Fig. 5C). However, to gain maximum accuracy in our estimates, we corrected the fluorescence ratios for the pH dependency of GEM-GECO1 (see Section 2.5 for details). After this calibration, we observed a strong correlation of mKeima and GEM-GECO1 fluorescence ratios (Fig. 5D, $R^2 = 0.85$) compared to the raw values (Fig. 5B, $R^2 = 0.22$). By employing the calibration curve (Fig. 4G), we determined that the luminal $Ca^{2+}$ concentration of the majority of endosomes is below 2 μM (Fig. 5D). The median $Ca^{2+}$ concentration was estimated to be ~900 nM, though this and all of our measured values lower than approximately 1 μM should be interpreted with caution as they are approaching the limits of quantification (LOQ) of the sensor pair as determined by *in vitro* calibration curves (Fig. 5D, Section 2)

While this analysis does reveal a high heterogeneity of endosomal $Ca^{2+}$ concentrations, essentially all endosomes display luminal $Ca^{2+}$ concentrations in the range between hundreds of nanomolar and 5 μM. These concentrations are within the range of cytoplasmic concentrations in many cell types under stimulated conditions [31], including human pancreatic beta-cells [32]. Interestingly, we observed a high correlation between pH and $Ca^{2+}$ content in the lumen of individual endosomes, with the endosomal $Ca^{2+}$ content increasing exponentially with decreasing pH (Fig. 5D). These data are consistent with a similar correlation reported for luminal pH and $Ca^{2+}$ in the lumen of lysosomes [33]. Thus, our genetically encoded biosensor pair enabled the first simultaneous semi-quantitative measurements of pH and $Ca^{2+}$ concentration in single endosomes of living cells. This approach provides a template for similar analyses in other acidic $Ca^{2+}$ handling organelles.

### 3.6. $Ca^{2+}$ flux into endosomes in glucose-stimulated beta-cells

Having characterized the heterogeneity of endosomal $Ca^{2+}$ under basal conditions, we next investigated the potential roles of endosomes in intracellular $Ca^{2+}$ homeostasis under physiological stimulation conditions. Glucose-stimulated insulin release from pancreatic beta-cells is strongly dependent on the influx of intracellular $Ca^{2+}$ through voltage-gated $Ca^{2+}$ channels in the plasma membrane [34,35]. However, chronically elevated cytoplasmic $Ca^{2+}$ can also induce cell death [36], making the control of these $Ca^{2+}$ influx signals critical. We previously hypothesized that organelles close to the plasma membrane may buffer the influx of $Ca^{2+}$ within beta-cells during glucose stimulation [37]. Our conclusion that $Ca^{2+}$ concentrations within some endosomal lumina are not very far from the cytosolic concentrations, prompted us to test this hypothesis by measuring real-time changes in

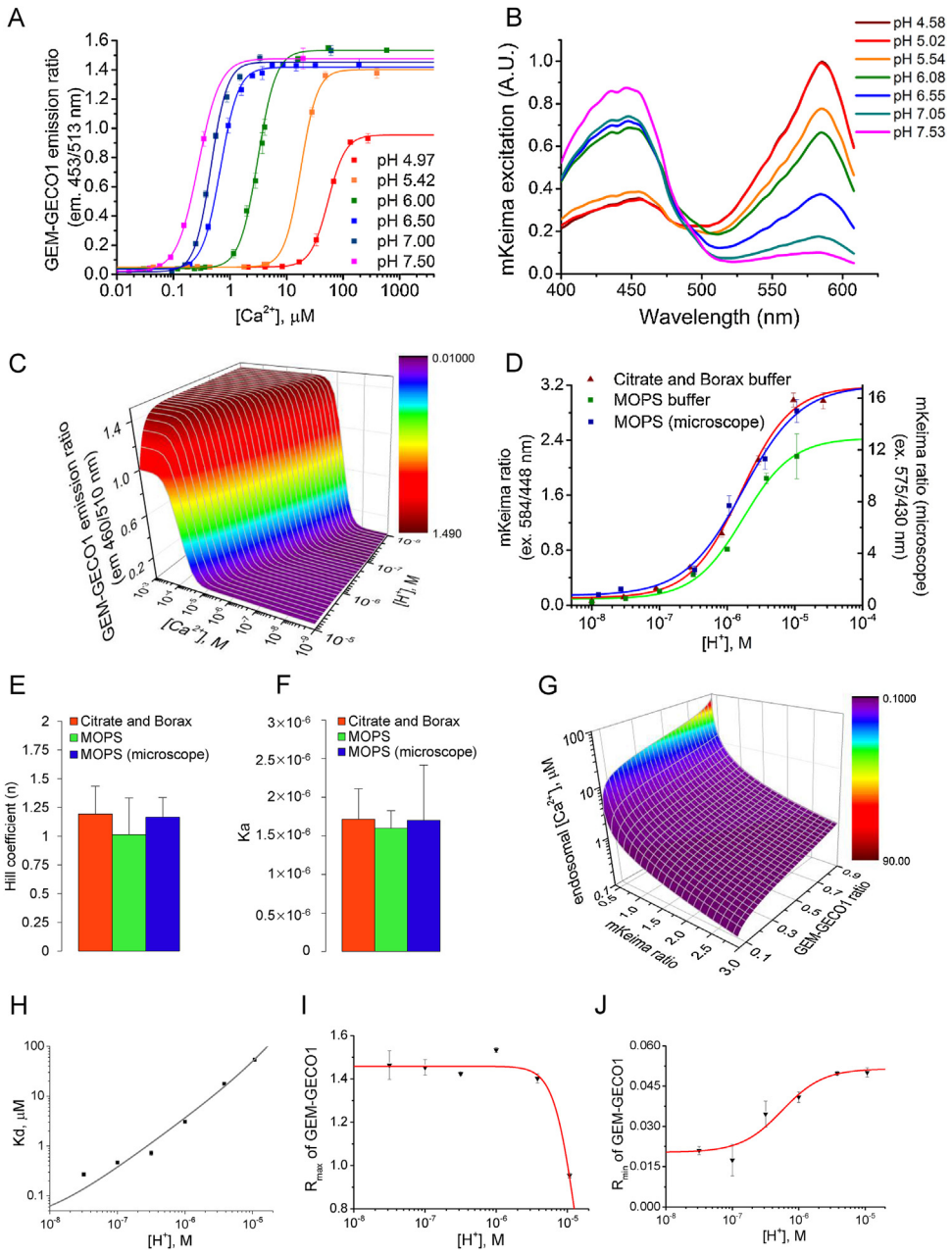


**Fig. 4.** Quantitative $Ca^{2+}$ measurements and *in vitro* calibration. (A) Ratio of GEM-GECO1 as a function of the $Ca^{2+}$ concentration in different pH conditions. (B) Excitation spectra of mKeima in as a function of the pH. (C) Ratio of GEM-GECO1 as a function of $Ca^{2+}$ and $H^+$ concentration. (D) Results of pH titration of mKeima. mKeima protein was reconstituted in citrate/borax buffer or MOPS buffer. mKeima ratios were measured with a plate reader or microscope. (E, F) Statistical analysis of apparent Hill coefficient and $K_a$ of mKeima measured under different conditions. (G) Endosomal $Ca^{2+}$ concentration as a function of the mKeima and GEM-GECO1 ratios based on ratiometric measurements with the microscope setup. (H–J) Coefficient curve fitting using GEM-GECO1 ratios obtained by microscope measurements. (H) $K_d$ of GEM-GECO1 as a function of $H^+$ concentration. (I) $R_{max}$ of GEM-GECO1 as a function of $H^+$ concentration; (J) the $R_{min}$ of GEM-GECO1 as a function of $H^+$ concentration. Error bars represent SEM ($n = 3$).

endosomal $Ca^{2+}$ during glucose stimulation. Fluorescence imaging of TiVAMP–GEM-GECO1-positive endocytic vesicles after switching extracellular glucose from 3 mM to 20 mM revealed an elevation of $Ca^{2+}$ within endosomes (Figs. 6A and B). To further characterize this phenomenon, we co-expressed TiVAMP–GEM-GECO1 and the early endosomal marker TagRFP-Rab5a. Early endosomes were identified in the TagRFP channel and the GEM-GECO1 intensity ratios for these objects were tracked to analyze relative early endosomal $Ca^{2+}$ content. $Ca^{2+}$ increases were measured in single Rab5a-positive early endosomes upon glucose stimulation (Fig. 6C). Indeed, the average early endosomal $Ca^{2+}$ content increased under elevated glucose conditions. The change of endosomal $Ca^{2+}$ upon glucose stimulation was independent of the luminal pH, which remained constant while the endosomal $Ca^{2+}$ concentration doubled under these acute high glucose conditions (Fig. 6D). Interestingly, the endosomal $Ca^{2+}$ did not typically return to baseline immediately after the return to non-stimulatory glucose after stimulation, possibly supporting the concept that a sub-population of endosomes may act as relatively long-acting $Ca^{2+}$ buffers. These data were supported by endosomal $Ca^{2+}$ measurements in a single glucose-stimulated human beta-cell (Fig. 6E). Together, these data suggest that a population of endosomes may act as a previously unappreciated component of the beta-cell $Ca^{2+}$ handling network during the glucose response.

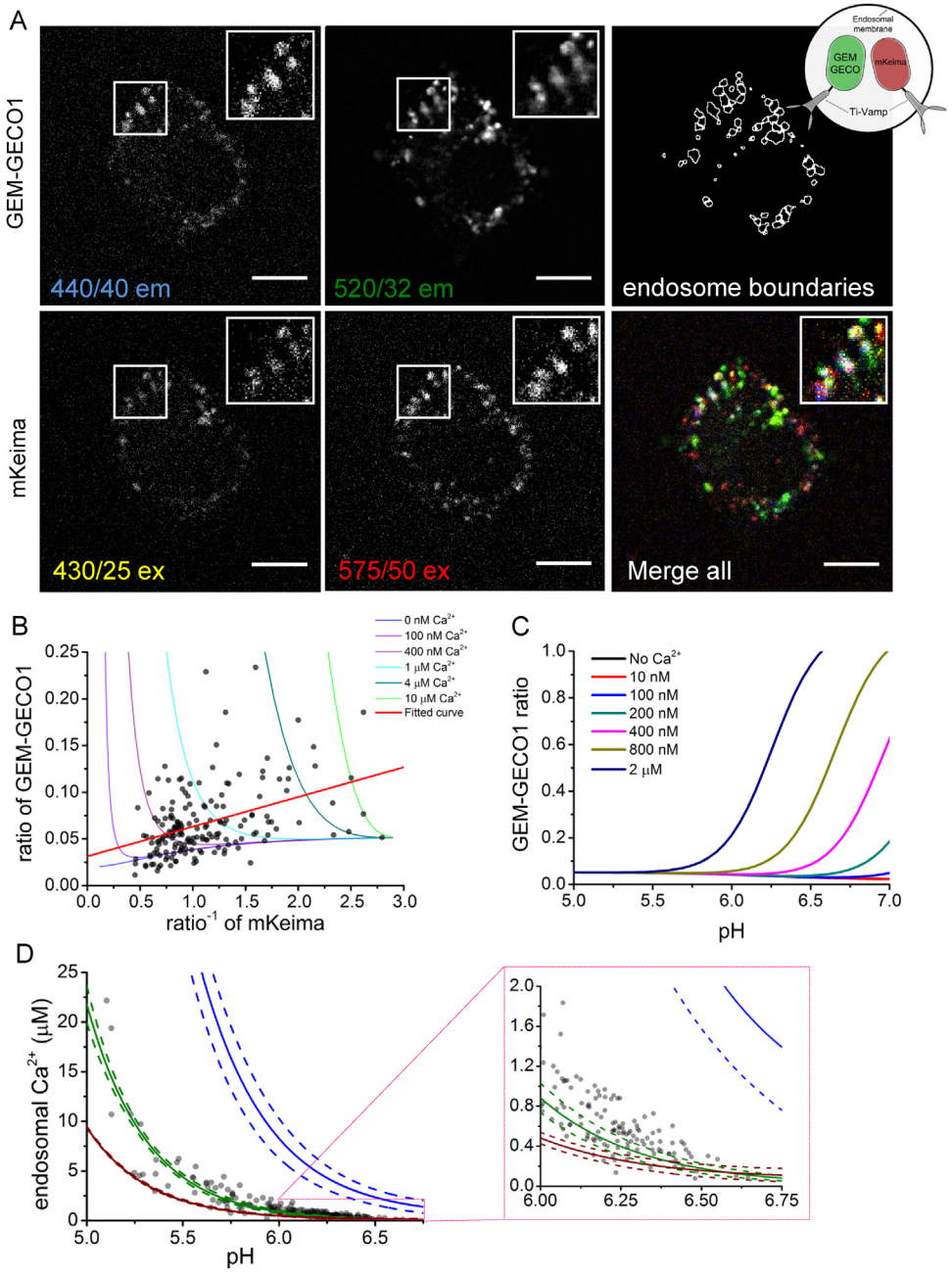


**Fig. 5.** Correlation between endosomal pH and $Ca^{2+}$. (A) Simultaneous imaging of mKeima and GEM-GECO1 targeted to the same population of endosomes. The merge panel shows the combined merge of 2 ratios (mKeima and GEM-GECO1) according to the 4 colors shown at the bottom of each panel. Inset is a schematic illustration of specific targeting of GEM-GECO1 and mKeima to the endosomal lumen for quantitative $Ca^{2+}$ and pH measurement *in situ*. (B) Raw single endosomal mKeima and GEM-GECO1 fluorescence ratios (6 cells). (C) Theoretical change of GEM-GECO1 ratio at different pH values and given $[Ca^{2+}]$. (D) Data from (B) following conversion to pH and $[Ca^{2+}]$ based on *in vitro* calibration curves. Green line represents a fitted equation of the form $[Ca^{2+}]_{free}$ (µM) $\approx 2 \times 10^{-6} \times 0.041^{pH}$, relating endosomal $Ca^{2+}$ and pH ($R^2 = 0.833$). Red and blue lines indicate the upper and lower limit of quantification (LOQ), with dashed lines representing the 95% confidence band. Note that our fitted curve is close to the lower limit of quantification. The median endosomal $[Ca^{2+}]$ was estimated to be ~0.9 µM and the average pH to be 6.05. Calculations are based on the analysis of 197 endosomes in 6 cells. Inset diagram shows enlarged area of the main diagram.

## 4. Discussion

The goal of the present study was to develop a pH-resistant $Ca^{2+}$ biosensor to directly measure $Ca^{2+}$ concentration in single endosomes and to determine whether endosomes play any role in pancreatic beta-cell $Ca^{2+}$ homeostasis. To accomplish these goals, we paired the GEM-GECO1 fluorescent $Ca^{2+}$ probe with the pH-sensitive mKeima fluorescent protein, and targeted both proteins to the luminal side of a defined sub-population of endosomes. Our semi-quantitative estimations suggest that $Ca^{2+}$ levels within the majority of endosomes are below 2 µM, in the range of cytoplasmic $Ca^{2+}$ levels observed in physiologically stimulated beta-cells, and orders of magnitude lower than what has previously been suggested from experiments using dyes taken up into endosomal compartments that were not molecularly defined [38]. We found endosomal $Ca^{2+}$ was higher in more acidic Rab7-positive late endosomes when compared with Rab5a-positive early endosomes. Our results also identify Rab5a-positive early endosomes as an organelle

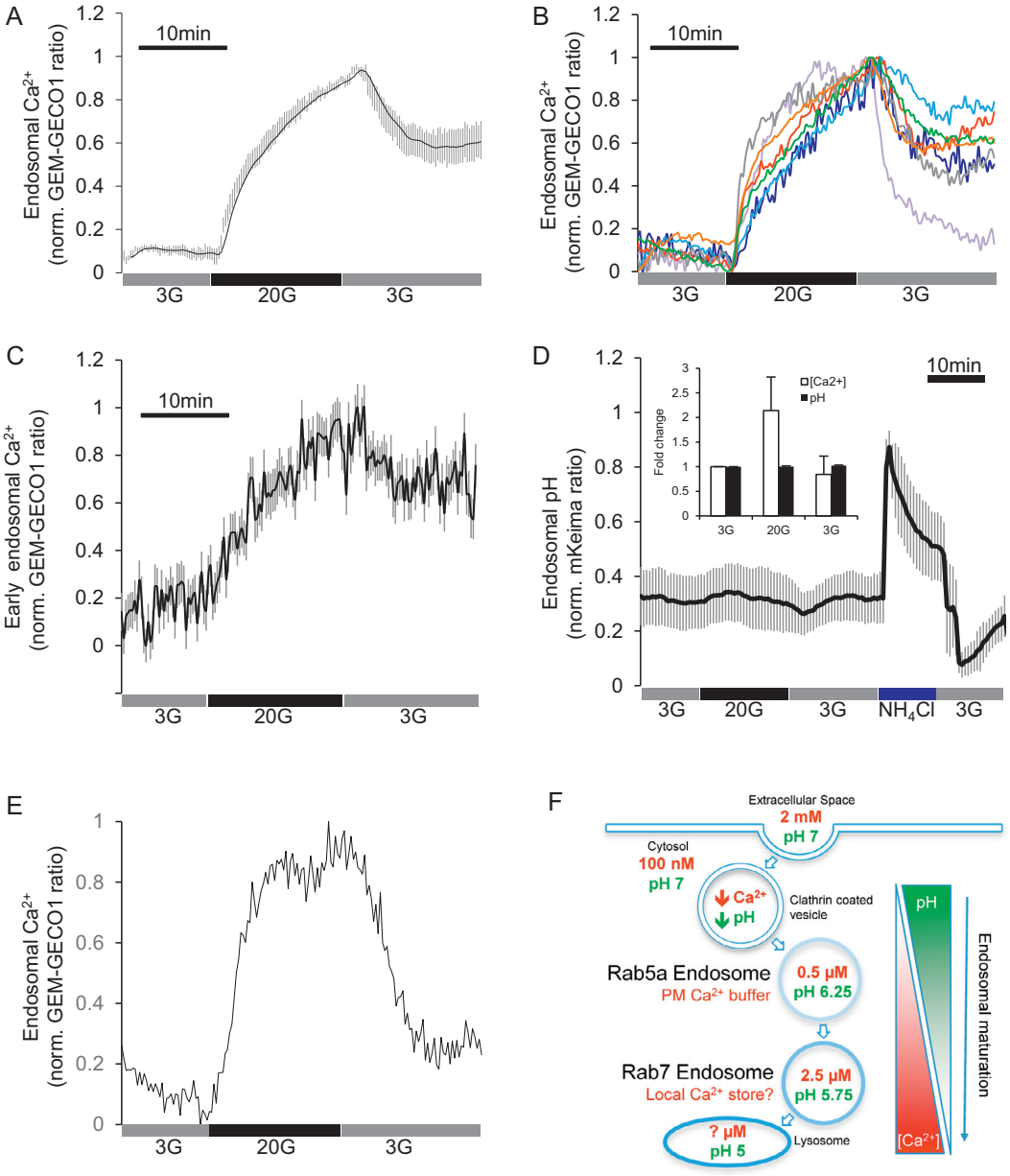


**Fig. 6.** Early endosomes enrich $Ca^{2+}$ in glucose-stimulated beta-cells. (A, B) Average and individual whole-cell endosomal $Ca^{2+}$ content in response to glucose ($n = 8$). (C) Early, Rab5a-positive endosomes were analyzed for their relative $Ca^{2+}$ content in response to glucose. (D) Average whole-cell endosomal pH in response to glucose. 20 mM $NH_4Cl$ was perfused as a positive control for mKeima ($n = 4$). (D, inset) Relation between endosomal pH and calcium content in the glucose response of a beta-cell ($n = 3$). Error bars represent SEM. (E) Average whole-cell endosomal $Ca^{2+}$ content in response to glucose in a human pancreatic beta-cell. (F) Working model of endosomal acidification and luminal $Ca^{2+}$ accumulation during organelle maturation. Measurements are only available for vesicles containing TiVAMP, Rab5a or Rab7.

compartment that can actively enrich $Ca^{2+}$ in glucose-stimulated beta-cells, demonstrating a previously unappreciated role for these organelles in intracellular $Ca^{2+}$ handling in pancreatic beta-cells.

Specific and quantitative data describing the luminal $Ca^{2+}$ concentrations within the endolysosmal organelle system has been hampered by a lack of appropriate molecular tools. Early pioneering work by Gerasimenko and colleagues relied on Oregon Green488 BAPTA-5 N taken up into cells from the extracellular media, to estimate a $Ca^{2+}$ concentration of ~28 μM in 'early' endosomes (defined as those imaged within 3 min after endocytosis). As the endosomes matured, the $Ca^{2+}$ was seen to drop to 8.5 μM 5 min after endocytosis, and then 3 μM 20 min after endocytosis [38]. On the other hand, Christensen et al. reported $Ca^{2+}$ levels of 400–600 μM in lysosome-like structures loaded with FFP18-AM, a dye reported to label cell membranes [33]. Previous work has addressed $Ca^{2+}$ release from isolated, artificially enlarged endolysosomal organelles [39,40], but whether this system approximates the situation in an intact cell remains unclear. The apparent lack of consensus between all of the described studies addressing the homeostasis of luminal endosomal $Ca^{2+}$ in intact cells clearly highlights the requirement for new biological tools that are able to specifically quantify endosomal $Ca^{2+}$ in living, fully functional cells. In the present study, we estimated $Ca^{2+}$ and pH within a molecularly defined sub-population of endosomes in living cells for the first time using genetically encoded biosensors.

One drawback of our genetically encoded protein-based $Ca^{2+}$ biosensor is that it was apparently unable to capture luminal $Ca^{2+}$ fluxes immediately after the initial moment of endosome internalization, when $Ca^{2+}$ would be equivalent to that in the bulk extracellular space. Our TiVAMP-targeted biosensor was unable to

capture this event, presumably due to the time required to recruit sufficient biosensor proteins to these nascent endosomes and/or due to the potential saturation of the $Ca^{2+}$ sensor at extremely high $Ca^{2+}$ concentrations. This property of our sensor contributes to an estimated average $Ca^{2+}$ concentration in our measured sub-population of endosomes that is lower than that previously proposed for endosomes including the $Ca^{2+}$ enriched nascent endosomes which are not included in our analysis. Approaches wherein $Ca^{2+}$ sensitive dyes are internalized directly from the extracellular space would be expected to capture this event and its immediate sequelae, so it is not surprising that those methods estimated high $Ca^{2+}$.

We demonstrated that our biosensor pair of TiVAMP–GEM-GECO1 and TiVAMP–mKeima can be used simultaneously to quantify the pH and the absolute $Ca^{2+}$ concentration in single endosomes. Control experiments demonstrated that TiVAMP–GEM-GECO1 responds primarily to $Ca^{2+}$ and only to pH to a lesser degree. Using this biosensor pair, we identified a remarkable heterogeneity of endosomal $Ca^{2+}$ content in beta-cells. We determined that this heterogeneity of endosomal $Ca^{2+}$ is associated with organelle maturation and acidification. Specifically, later endosomes with lower luminal pH have higher endosomal $Ca^{2+}$ concentrations (Fig. 6F). Interestingly, a correlation between $Ca^{2+}$ and pH in endocytic vesicles mediated by a pH-sensitive $Ca^{2+}$ channel has been suggested [41]. It was further shown by others that a disruption of endosomal $Ca^{2+}$ homeostasis leads to a disruption of the endolysosomal transport system, supporting the concept of $Ca^{2+}$ as a central regulator in membrane fusion and endosome acidification [41]. Together with work from other groups, our data suggest a strong interrelationship of $Ca^{2+}$ and pH within the endolysosomal system [33], but further work is needed to firmly establish the causal relationship between $Ca^{2+}$ flux and pH in these organelle lumina.

Live-cell, intra-organelle $Ca^{2+}$ imaging is a powerful approach to understanding the fundamental biology of endosomes and other organelles [4]. The GEM-GECO1 probe has been extensively tested *in vitro* where it exhibits robust ratiometric $Ca^{2+}$ sensing, with sufficient dynamic range and relative pH insensitivity [16]. GEM-GECO1 is significantly smaller than previous biosensors based on $Ca^{2+}$-dependent FRET between two fluorescent proteins. We propose that the combined use of endosome-targeted GEM-GECO1 and mKeima marks a significant improvement over alternate approaches. Together with this previous work [26], our data demonstrate that linking GEM-GECO1 to TiVAMP permits high localization specificity, to an extent that is not possible with dye-based approaches [42].

The imaging approach described in this work attempts to achieve the very challenging goal of simultaneously quantifying both endosomal pH and $Ca^{2+}$ using the most appropriate combination of spectrally distinct genetically encoded sensors currently available. Relative to the use of dye-based indictors, genetically encoded biosensors have the advantage of being less invasive and also enabling the targeting of organelles with molecular specificity (*i.e.*, Rab5a *vs.* Rab7 endosomes). However, the imaging approach used in this work also has a number of limitations that place constraints on the accuracy, temporal resolution, and the lower limit of quantification that can be achieved. A major challenge of this work is accounting for the fact that the GEM-GECO1 $Ca^{2+}$ indicator has both a fluorescence response and a $Ca^{2+}$ affinity that is still somewhat pH dependent. To correct for these dependencies, we projected an *in vitro* calibration onto a dataset of cellular measurements. This procedure required multiple assumptions – the most important of which was the assumption that the *in vitro* $K_d$ is maintained in cells. It is not known whether our probe would have identical properties in an *in situ* calibration. Another challenge was related to the fact that individual endosomes are small structures that have relatively low signal-to-noise for single measurements, and the fact that cellular autofluorescence at the wavelengths used for imaging was substantial and could only be corrected using a sophisticated local background subtraction technique. With respect to temporal resolution, our ratiometric sensor pair requires the acquisition of 4 fluorescence emission channels, and so our ability to image rapid endosomal $Ca^{2+}$ and pH fluxes is limited by the exposure times and sensitivity of the imaging system. Taking these caveats into consideration, we are more confident about the upper range of our estimates of endosomal $Ca^{2+}$ concentration than we are of the lower end of the range. However, we note that our measurements of endosomal $Ca^{2+}$ and pH do fit within a range of concentrations proposed in previous studies [33,38]. We anticipate that combined use of GEM-GECO1 and mKeima will prove useful for simultaneous semi-quantitative measurements of $Ca^{2+}$ and pH in the lumina of other organelles. For example, it should be feasible to link GEM-GECO1 and mKeima to SNARE proteins of the exocytotic machinery to study pH and $Ca^{2+}$ dynamics within secretory granules, possibly providing new insight into the role of luminal $Ca^{2+}$ in exocytotic events [43,44].

Our results provide an improved understanding of dynamic $Ca^{2+}$ homeostasis in beta-cells and, as such, take a step toward further elucidating the physiological control of insulin secretion and other $Ca^{2+}$-dependent processes in this key endocrine cell type [2,6,32,45]. In response to elevated extracellular glucose levels, cytoplasmic $Ca^{2+}$ levels increase to drive the docking and fusion of secretory insulin granules with the plasma membrane of the beta cell [35]. Interestingly, alterations in beta-cell $Ca^{2+}$ homeostasis have been implicated in the development of type 2 diabetes [46]. Specifically, it has been proposed that excessive $Ca^{2+}$ influx leads to an increased beta-cell death by apoptosis, a phenomenon associated with diabetes [47]. In this context, we previously speculated that endosomes might act as $Ca^{2+}$ buffers in beta-cells responding to high glucose [37]. In the present work, we provided experimental data that are consistent with this model.

The degree to which endosomes contribute to the total $Ca^{2+}$ buffering ability of intracellular organelles remains to be elucidated. Endosomes occupy a small volume of many cell types (0.65–2%), but this may be higher in beta-cells. We speculate that endosomes may play a role as physiologically relevant local $Ca^{2+}$ buffers only near the plasma membrane, shaping $Ca^{2+}$ signals that originate in close proximity. Unlike larger $Ca^{2+}$-handling organelles such as mitochondria (3.9% of the total beta-cell volume) or ER (20% of the total beta-cell volume) [48–50], endosomes may not play a primary role in shaping $Ca^{2+}$ signals originating from within the cell. Our novel endosomal $Ca^{2+}$ biosensor promises to shed light on the mechanisms involved in endosomal $Ca^{2+}$ homeostasis in intact living cells and resolve current controversies around the nature of this important organelle [39,40,51].

## Author contributions

Tobias Albrecht, Yongxin Zhao and Trang Hai Nguyen performed experiments. Tobias Albrecht, Yongxin Zhao, Robert E. Campbell and James D. Johnson designed experiments, analyzed data and wrote the manuscript. James D. Johnson is the guarantor of this work.

## Acknowledgements

We thank the University of Alberta MBSU for technical assistance. pmKeima-Red-N1 vector is a gift from Michael Davidson. peGFP-C3-TiVAMP was a gift from Thierry Galli. This work was supported by a CIHR Catalyst Grant NHG 99085 to R.E.C. and J.D.J, an NSERC Grant RGPIN 288338 to R.E.C., and a CIHR Operating Grant MOP-133692 to J.D.J. T.A. was supported by a scholarship from the

German Hans Sauer Stiftung and Y.Z. was supported by a scholarship from Alberta Innovates. R.E.C. holds a Tier II Canada Research Chair in Bioanalytical Chemistry.

## References


[1] D.E. Clapham, Calcium signaling, Cell 131 (2007) 1047–1058.
[2] J.D. Johnson, M.J. Bround, S.A. White, D.S. Luciani, Nanospaces between endoplasmic reticulum and mitochondria as control centres of pancreatic beta-cell metabolism and survival, Protoplasma 249 (Suppl. 1) (2012) S49–S58.
[3] J.D. Johnson, J.P. Chang, Function- and agonist-specific $Ca^{2+}$ signalling: the requirement for and mechanism of spatial and temporal complexity in $Ca^{2+}$ signals, Biochem. Cell Biol. 78 (2000) 217–240.
[4] L. Lindenburg, M. Merkx, Colorful calcium sensors, Chembiochem 13 (2012) 349–351.
[5] N. Demaurex, M. Frieden, Measurements of the free luminal ER Ca(2+) concentration with targeted cameleon fluorescent proteins, Cell Calcium 34 (2003) 109–119.
[6] D.S. Luciani, K.S. Gwiazda, T.L. Yang, T.B. Kalynyak, Y. Bychkivska, M.H. Frey, K.D. Jeffrey, A.V. Sampaio, T.M. Underhill, J.D. Johnson, Roles of IP3R and RyR $Ca^{2+}$ channels in endoplasmic reticulum stress and beta-cell death, Diabetes 58 (2009) 422–432.
[7] L.M. Traub, S. Kornfeld, The trans-Golgi network: a late secretory sorting station, Curr. Opin. Cell Biol. 9 (1997) 527–533.
[8] P. Pizzo, V. Lissandron, P. Capitanio, T. Pozzan, Ca(2+) signalling in the Golgi apparatus, Cell Calcium 50 (2011) 184–192.
[9] S. Patel, S. Muallem, Acidic Ca(2+) stores come to the fore, Cell Calcium 50 (2011) 109–112.
[10] C. Brownlee, Cellular calcium imaging: so, what's new? Trends Cell Biol. 10 (2000) 451–457.
[11] H.W. Platta, H. Stenmark, Endocytosis and signaling, Curr. Opin. Cell Biol. 23 (2011) 393–403.
[12] K.S. Gwiazda, T.L. Yang, Y. Lin, J.D. Johnson, Effects of palmitate on ER and cytosolic $Ca^{2+}$ homeostasis in beta-cells, American journal of physiology, Endocrinol. Metab. 296 (2009) E690–E701.
[13] M.R. Alam, L.N. Groschner, W. Parichatikanond, L. Kuo, A.I. Bondarenko, R. Rost, M. Waldeck-Weiermair, R. Malli, W.F. Graier, Mitochondrial $Ca^{2+}$ uptake 1 (MICU1) and mitochondrial $Ca^{2+}$ uniporter (MCU) contribute to metabolism-secretion coupling in clonal pancreatic beta-cells, J. Biol. Chem. 287 (2012) 34445–34454.
[14] J. Nakai, M. Ohkura, K. Imoto, A high signal-to-noise Ca(2+) probe composed of a single green fluorescent protein, Nat. Biotechnol. 19 (2001) 137–141.
[15] J. Akerboom, T.W. Chen, T.J. Wardill, L. Tian, J.S. Marvin, S. Mutlu, N.C. Calderon, F. Esposti, B.G. Borghuis, X.R. Sun, A. Gordus, M.B. Orger, R. Portugues, F. Engert, J.J. Macklin, A. Filosa, A. Aggarwal, R.A. Kerr, R. Takagi, S. Kracun, E. Shigetomi, B.S. Khakh, H. Baier, L. Lagnado, S.S. Wang, C.I. Bargmann, B.E. Kimmel, V. Jayaraman, K. Svoboda, D.S. Kim, E.R. Schreiter, L.L. Looger, Optimization of a GCaMP calcium indicator for neural activity imaging, J. Neurosci. 32 (2012) 13819–13840.
[16] Y. Zhao, S. Araki, J. Wu, T. Teramoto, Y.-F. Chang, M. Nakano, A.S. Abdelfattah, M. Fujiwara, T. Ishihara, T. Nagai, R.E. Campbell, An expanded palette of genetically encoded $Ca^{2+}$ indicators, Science 333 (2011) 1888–1891.
[17] S. Bolte, F.P. Cordelieres, A guided tour into subcellular colocalization analysis in light microscopy, J. Microsc. 224 (2006) 213–232.
[18] A.E. Carpenter, T.R. Jones, M.R. Lamprecht, C. Clarke, I.H. Kang, O. Friman, D.A. Guertin, J.H. Chang, R.A. Lindquist, J. Moffat, P. Golland, D.M. Sabatini, CellProfiler: image analysis software for identifying and quantifying cell phenotypes, Genome Biol. 7 (2006) R100.
[19] J. Schindelin, I. Arganda-Carreras, E. Frise, V. Kaynig, M. Longair, T. Pietzsch, S. Preibisch, C. Rueden, S. Saalfeld, B. Schmid, J.Y. Tinevez, D.J. White, V. Hartenstein, K. Eliceiri, P. Tomancak, A. Cardona, Fiji: an open-source platform for biological-image analysis, Nat. Methods 9 (2012) 676–682.
[20] S.R. Sternberg, Biomedical image-processing, Computer 16 (1983) 22–34.
[21] G. Grynkiewicz, M. Poenie, R.Y. Tsien, A new generation of $Ca^{2+}$ indicators with greatly improved fluorescence properties, J. Biol. Chem. 260 (1985) 3440–3450.
[22] D.M. Bers, C.W. Patton, R. Nuccitelli, A practical guide to the preparation of $Ca^{2+}$ buffers, Methods Cell Biol. 40 (1994) 3–29.
[23] P.R. Pryor, B.M. Mullock, N.A. Bright, M.R. Lindsay, S.R. Gray, S.C. Richardson, A. Stewart, D.E. James, R.C. Piper, J.P. Luzio, Combinatorial SNARE complexes with VAMP7 or VAMP8 define different late endocytic fusion events, EMBO Rep. 5 (2004) 590–595.
[24] R.J. Advani, B. Yang, R. Prekeris, K.C. Lee, J. Klumperman, R.H. Scheller, VAMP-7 mediates vesicular transport from endosomes to lysosomes, J. Cell Biol. 146 (1999) 765–776.
[25] S. Martinez-Arca, R. Rudge, M. Vacca, G. Raposo, J. Camonis, V. Proux-Gillardeaux, L. Daviet, E. Formstecher, A. Hamburger, F. Filippini, M. D'Esposito, T. Galli, A dual mechanism controlling the localization and function of exocytic v-SNAREs, Proc. Natl. Acad. Sci. U. S. A. 100 (2003) 9011–9016.
[26] S. Martinez-Arca, P. Alberts, A. Zahraoui, D. Louvard, T. Galli, Role of tetanus neurotoxin insensitive vesicle-associated membrane protein (TI-VAMP) in vesicular transport mediating neurite outgrowth, J. Cell Biol. 149 (2000) 889–900.
[27] J. Rink, E. Ghigo, Y. Kalaidzidis, M. Zerial, Rab conversion as a mechanism of progression from early to late endosomes, Cell 122 (2005) 735–749.
[28] J. Huotari, A. Helenius, Endosome maturation, EMBO J. 30 (2011) 3481–3500.
[29] S. Violot, P. Carpentier, L. Blanchoin, D. Bourgeois, Reverse pH-dependence of chromophore protonation explains the large Stokes shift of the red fluorescent protein mKeima, J. Am. Chem. Soc. 131 (2009) 10356–10357.
[30] K.D. Piatkevich, J. Hulit, O.M. Subach, B. Wu, A. Abdulla, J.E. Segall, V.V. Verkhusha, Monomeric red fluorescent proteins with a large Stokes shift, Proc. Natl. Acad. Sci. U. S. A. 107 (2010) 5369–5374.
[31] E. Zampese, P. Pizzo, Intracellular organelles in the saga of $Ca^{2+}$ homeostasis: different molecules for different purposes? Cell. Mol. Life Sci. 69 (2012) 1077–1104.
[32] J.D. Johnson, S. Misler, Nicotinic acid-adenine dinucleotide phosphate-sensitive calcium stores initiate insulin signaling in human beta cells, Proc. Natl. Acad. Sci. U. S. A. 99 (2002) 14566–14571.
[33] K.A. Christensen, J.T. Myers, J.A. Swanson, pH-dependent regulation of lysosomal calcium in macrophages, J. Cell Sci. 115 (2002) 599–607.
[34] S. Misler, D.W. Barnett, K.D. Gillis, D.M. Pressel, Electrophysiology of stimulus-secretion coupling in human beta-cells, Diabetes 41 (1992) 1221–1228.
[35] M. Sakurada, A. Kanatsuka, T. Saitoh, H. Makino, K. Yamamura, J. Miyazaki, M. Kikuchi, S. Yoshida, Relation between glucose-stimulated insulin secretion and intracellular calcium accumulation studied with a superfusion system of a glucose-responsive pancreatic beta-cell line MIN6, Endocrinology 132 (1993) 2659–2665.
[36] S. Orrenius, B. Zhivotovsky, P. Nicotera, Regulation of cell death: the calcium-apoptosis link, Nat. Rev. Mol. Cell Biol. 4 (2003) 552–565.
[37] J.D. Johnson, S. Kuang, S. Misler, K.S. Polonsky, Ryanodine receptors in human pancreatic beta cells: localization and effects on insulin secretion, FASEB J. 18 (2004) 878–880.
[38] J.V. Gerasimenko, A.V. Tepikin, O.H. Petersen, O.V. Gerasimenko, Calcium uptake via endocytosis with rapid release from acidifying endosomes, Curr. Biol. 8 (1998) 1335–1338.
[39] P.J. Calcraft, M. Ruas, Z. Pan, X. Cheng, A. Arredouani, X. Hao, J. Tang, K. Rietdorf, L. Teboul, K.-T. Chuang, P. Lin, R. Xiao, C. Wang, Y. Zhu, Y. Lin, C.N. Wyatt, J. Parrington, J. Ma, A.M. Evans, A. Galione, M.X. Zhu, NAADP mobilizes calcium from acidic organelles through two-pore channels, Nature 459 (2009) 596–600.
[40] X. Wang, X. Zhang, X.P. Dong, M. Samie, X. Li, X. Cheng, A. Goschka, D. Shen, Y. Zhou, J. Harlow, M.X. Zhu, D.E. Clapham, D. Ren, H. Xu, TPC proteins are phosphoinositide-activated sodium-selective ion channels in endosomes and lysosomes, Cell 151 (2012) 372–383.
[41] B. Lelouvier, R. Puertollano, Mucolipin-3 regulates luminal calcium, acidification, and membrane fusion in the endosomal pathway, J. Biol. Chem. 286 (2011) 9826–9832.
[42] M. Kamiya, K. Johnsson, Localizable and highly sensitive calcium indicator based on a BODIPY fluorophore, Anal. Chem. 82 (2010) 6472–6479.
[43] A. Raveh, M. Valitsky, L. Shani, J.R. Coorssen, P.S. Blank, J. Zimmerberg, R. Rahamimoff, Observations of calcium dynamics in cortical secretory vesicles, Cell Calcium 52 (2012) 217–225.
[44] E.J. Dickson, J.G. Duman, M.W. Moody, L. Chen, B. Hille, Orai-STIM-mediated $Ca^{2+}$ release from secretory granules revealed by a targeted $Ca^{2+}$ and pH probe, Proc. Natl. Acad. Sci. U. S. A. 109 (2012) E3539–E3548.
[45] V. Dror, T.B. Kalynyak, Y. Bychkivska, M.H. Frey, M. Tee, K.D. Jeffrey, V. Nguyen, D.S. Luciani, J.D. Johnson, Glucose and endoplasmic reticulum calcium channels regulate HIF-1beta via presenilin in pancreatic beta-cells, J. Biol. Chem. 283 (2008) 9909–9916.
[46] P. Rorsman, M. Braun, Q. Zhang, Regulation of calcium in pancreatic alpha- and beta-cells in health and disease, Cell Calcium 51 (2012) 300–308.
[47] J.D. Johnson, D.S. Luciani, Mechanisms of pancreatic beta-cell apoptosis in diabetes and its therapies, Adv. Exp. Med. Biol. 654 (2010) 447–462.
[48] P.M. Dean, Ultrastructural morphometry of the pancreatic beta-cell, Diabetologia 9 (1973) 115–119.
[49] P. Marbet, C. Rahner, B. Stieger, L. Landmann, Quantitative microscopy reveals 3D organization and kinetics of endocytosis in rat hepatocytes, Microsc. Res. Tech. 69 (2006) 693–707.
[50] G. Griffiths, R. Back, M. Marsh, A quantitative analysis of the endocytic pathway in baby hamster kidney cells, J. Cell Biol. 109 (1989) 2703–2720.
[51] J.C. Hay, Calcium: a fundamental regulator of intracellular membrane fusion? EMBO Rep. 8 (2007) 236–240.
[52] P.C. Meier, R.E. Zünd, Statistical Methods in Analytical Chemistry, Wiley, New York, 1993, pp. 105.